Optimization of mixing in agitated reactors: A CFD-based approach for energy efficiency and dispersion in biphasic systems

José Alfredo Parra-Reyes [*], Isaac Salvador Cuevas Sosa, Adrián López Yáñez, Rafael Alejandro Ángel Cuapio, and Gastón Martínez-de-Jesús

[1] División de Ingeniería Química y Bioquímica, Tecnológico Nacional de México/ TES de Ecatepec, Av. Tecnológico S/N, Colonia. Valle de Anáhuac, Ecatepec de Morelos, C. P. 55210, Estado de México. México.
* Corresponding author: jalfred.parra.r.1@gmail.com; Tel.: +525567576919

Received: August 23, 2025 Accepted: October 2, 2025 Published: March 19, 2026
DOI: https://doi.org/10.56845/rebs.v8i1.675

Abstract: A Computational Fluid Dynamics (CFD) study was conducted to simulate the hydrodynamic behavior of a Norstone-type high-shear impeller operating in a stirred unbaffled tank containing a biphasic system (glycerin-hexane). A transient, multiphase Eulerian-Eulerian approach was implemented in ANSYS Fluent under laminar flow conditions. The model captured the formation of four distinct recirculation loops and identified zones of high-energy dissipation at the impeller blades, which are critical for the dispersion of the secondary phase. Experimental validation was conducted using temperature sensors (Max6675 thermocouples) connected to an Arduino Uno; good agreement between simulated and measured temperatures was observed. This work provides a validated CFD framework and fundamental insight into the flow dynamics, establishing a solid foundation for optimizing impeller geometry and operating conditions to achieve greater mixing homogeneity and energy efficiency in industrial biphasic systems**.**

Keywords: CFD, high-shear impeller, mixing efficiency, laminar flow, Euler–Euler model

Introduction

Optimizing industrial processes is a key strategy for enhancing operational efficiency and reducing environmental impact by rationalizing energy and resource use. In this context, stirred reactors, widely used in the pharmaceutical, chemical, and biotechnological industries, require a thorough analysis of their geometry, operating conditions, and governing hydrodynamics. Key hydrodynamic variables such as turbulent kinetic energy (TKE), velocity fields, circulation patterns, energy dissipation rates, and mixing times are essential for evaluating their performance and are necessary for assessing dispersion quality and system homogenization (Oshinowo L. & Marshall E., 2001).

Computational Fluid Dynamics (CFD) facilitates the analysis and optimization of these parameters through numerical simulations, reducing the need for extensive experimental studies. This approach provides a robust quantitative basis for improving mixing performance, optimizing energy consumption, and establishing reliable scale-up strategies (Stuparu *et al*., 2021). Moreover, its implementation can support the development of technologies aligned with circular economy principles, such as the valorization of agro-industrial residues to obtain high-value products (Obando-Galicia Y., 2024).

The thorough analysis of hydrodynamic variables using CFD has become a high-impact engineering tool, indispensable for the design and operation of efficient and sustainable mixing systems. This methodology is rooted in solving a model based on the conservation equations of mass and momentum, which form a coupled system of nonlinear partial differential equations. Since analytical solutions are possible only for highly simplified cases, CFD provides reliable approximations for complex engineering problems through specialized software, enabling the detailed analysis of hydrodynamic variables. The CFD approach applies the finite volume method to discretize the differential equations and transform them into a system of algebraic equations that can be solved using iterative methods (Andersson, 2012). The equations that describe the behavior of a multiphase system are the continuity equation (Eq. 1) and the momentum transfer equation (Eq. 2).

$$\frac{\partial}{\partial t}\left(\alpha_q \rho_q\right) + \nabla \cdot \left(\alpha_q \rho_q \vec{v}_q\right) = \sum_{p=1}^{n}\left(\dot{m}_{pq} - \dot{m}_{qp}\right) + S_q \quad \textbf{(1)}$$

$$\frac{\partial}{\partial t}\left(\alpha_q \rho_q \vec{v}_q\right) + \nabla \cdot \left(\alpha_q \rho_q \vec{v}_q \vec{v}_q\right) = -\alpha_q \nabla \mathrm{p} + \nabla \cdot \bar{\bar{\tau}}_q + \alpha_q \rho_q \vec{g} + \sum_{p=1}^{n}\left(\vec{R}_{pq} + \dot{m}_{pq}\vec{v}_{pq} - \dot{m}_{qp}\vec{v}_{qp}\right) + \left(\vec{F_q} + \vec{F}_{lift,q} + \vec{F}_{vm,q}\right) \quad \textbf{(2)}$$

where the stress tensor of each phase, $\bar{\bar{\tau}}_q$, is expressed by

$$\overline{\overline{\tau_q}} = \alpha_q \mu_q \left(\nabla \vec{v}_q + \nabla \vec{v}_q^T\right) + \alpha_q \left(\lambda_q - \frac{3}{2}\mu_q\right) \nabla \cdot \vec{v}_q \bar{\bar{\mathrm{I}}} \quad \textbf{(3)}$$

Here, α_q is thephase volume fraction, $\vec{v}_q$represents the velocity, ρ_q is the density of phase q; $\dot{m}_{pq}$and $\dot{m}_{qp}$denote the mass transfer terms between phases p and q. The coefficients $\mu_q$and $\lambda_q$correspond to the shear viscosity and the apparent viscosity of each phase, respectively. The q^{th} phase is subjected to several forces, including the external force $\vec{F}_q$, the lift force $\vec{F}_{lift,q}$, and the virtual mass force $\vec{F}_{vm,q}$. In addition, interphase interactions are governed by the interfacial force $\vec{R}_{pq}$, which depends on effects such as friction, pressure, and cohesion, and satisfies the symmetrical conditions $\vec{R}_{pq} = -\vec{R}_{qp}$and $\vec{R}_{qq} = 0$. All phases share the same pressure p, and the interfacial velocity between phases is denoted by $\vec{v}_{pq}$.

The energy conservation equation is incorporated, as given by Eq. 4.

$$\frac{\partial}{\partial \partial}(\rho E) + \nabla \cdot \left(\vec{v}(\rho E + p)\right) = \nabla \cdot \left(k_{eff} \nabla \mathrm{T} - \sum_q \sum_j h_{j,q} \vec{J}_{j,q} + \left(\bar{\bar{\tau}}_{eff} \cdot \vec{v}\right) \right) + s_h \quad \textbf{(4)}$$

where k_{eff} is the effective thermal conductivity $(k + k_t$, where k_t is the turbulent thermal conductivity defined according to the selected turbulence model), and $\vec{J}_j$ is the diffusion flux of species j. The first three terms on the right-hand side of Eq. (4) correspond to energy transfer by conduction, species diffusion, and viscous dissipation, respectively. S_h includes the volumetric heat source previously defined in the model.

In Eq. 5,

$$E = h - \frac{p}{\rho} + \frac{v^2}{2} \quad \textbf{(5)}$$

where sensible enthalpy h is defined for incompressible flows as

$$h = \sum_j Y_j h_j + \frac{p}{\rho} \quad \textbf{(6)}$$

Y_j is the mass fraction of species *j* and

$$h_j = \int_{T_{ref}}^{T} C_{p,j}\, dT \quad \textbf{(7)}$$

(ANSYS, 2016).

In this study, CFD approach was used to characterize the hydrodynamics of biphasic mixing systems, evaluating key parameters to guide the optimization of industrial reactor design and operation.

Materials and Methods

*T*he mixing system consisted of a high a shear impeller (Norstone® model, Norstone Inc., PA), based on the patent by Steinmetz (1993) and an unbaffled flat-bottomed glass tank. The dimensions of the impeller were diameter (D) of 49 mm, height (h) of 6 mm, and groove diameter of 3 mm, as shown in Figure 1a. The mixing tank had a diameter (T) of

142 mm. The impeller was set at a C/T ratio of 0.73, where C is the distance from the bottom of the tank to the impeller center (Figure 1b).

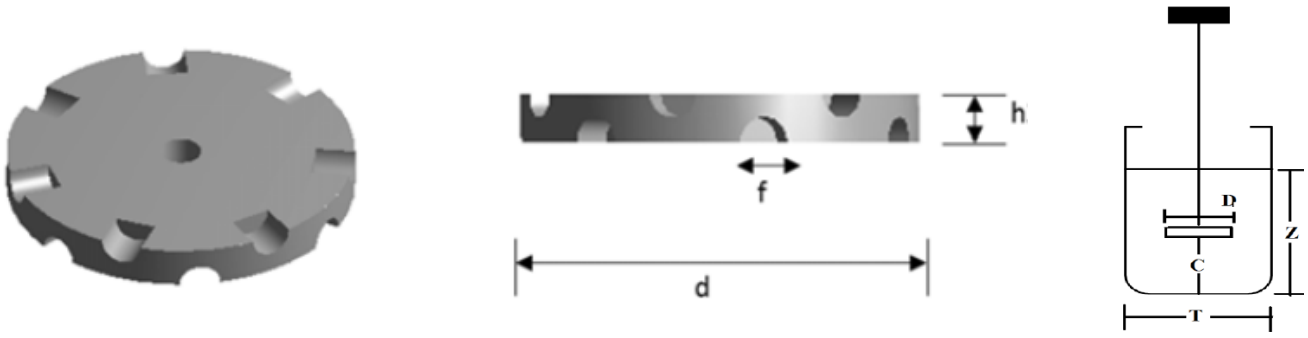

Figure 1. (a) Geometry impeller, (b) Geometry reactor

The stirred tank was modeled using ANSYS Fluent v. 2024 R1 (Student) (ANSYS, Inc., 2024). The geometry was generated in the DesignModeler module, and the computational mesh was built in the Meshing module, both in ANSYS Workbench. The model solved the governing conservation equations for mass and momentum. The simulations were performed on a laptop with an Intel Core i5-13420H processor running at 2.10 GHz, 16 GB of RAM, and an NVIDIA GeForce RTX 4050 graphics card.

The simulation was performed under transient conditions with a time step of 0.001 s. To represent the multiphase nature of the system, the Eulerian–Eulerian model was employed under a laminar flow formulation. The impeller rotation was simulated using the Multiple Reference Frame (MRF) approach. In this approach, the rotating region is approximated as a quasi-steady state to obtain the mean rotational field at a lower computational cost (Deglon & Meyer, 2006). It should be noted that, due to its inherent limitations, the MRF approach does not reproduce transient rotor–stator interactions; therefore, the reported quantities must be interpreted as averages or approximations of the rotational field in a pseudo-steady regime. The region surrounding the impeller (RRF), a cylinder of radius 35 mm and height of 16 mm, was assumed to rotate at 280 RPM. A standard pressure–velocity coupling scheme was used, together with the QUICK discretization scheme. The shaft and the impeller were considered rotating walls at the same velocity as RRF. The no-slip condition was applied to the tank wall.

For experimental validation, two temperature sensors (Max6675 thermocouples) were connected to an Arduino Uno microcontroller. The sensors were installed on the inner tank walls at two different heights: Sensor 1 at 45 mm and Sensor 2 at 115 mm from the bottom. Validation was performed by comparing simulation results with experimental data using temperature-versus-time graphs. The working fluid was glycerin at 23 °C; its viscosity (1.2 Pa·s) was determined using an MCR 72 Anton Paar rheometer, and its density (1260 kg m^{-3}) was determined by using a graduated cylinder and an analytical balance. Hexane at 50 °C was used as the second phase at a mass fraction of 20%.

Results and Discussion

The temperature evolution during the initial seconds of the process was analyzed experimentally, as this stage exhibits the highest rate of heat transfer. This behavior was then compared with the results obtained from the CFD simulations, as shown in Figure 2. The differences between the curves obtained from the simulations and those measured experimentally were minimal, suggesting that the CFD model accurately reproduces the observed thermal behavior. Jadhav and Barigou (2022) studied a 3D Eulerian-Lagrangian CFD model to simulate the turbulent flow and mixing of coarse dense particles in a standard batch vessel, mechanically agitated by a down-pumping pitched-blade turbine. Their numerical results were experimentally validated using positron emission particle tracking. Both datasets show very good agreement. Our results suggest that it is possible to validate CFD results with simple techniques.

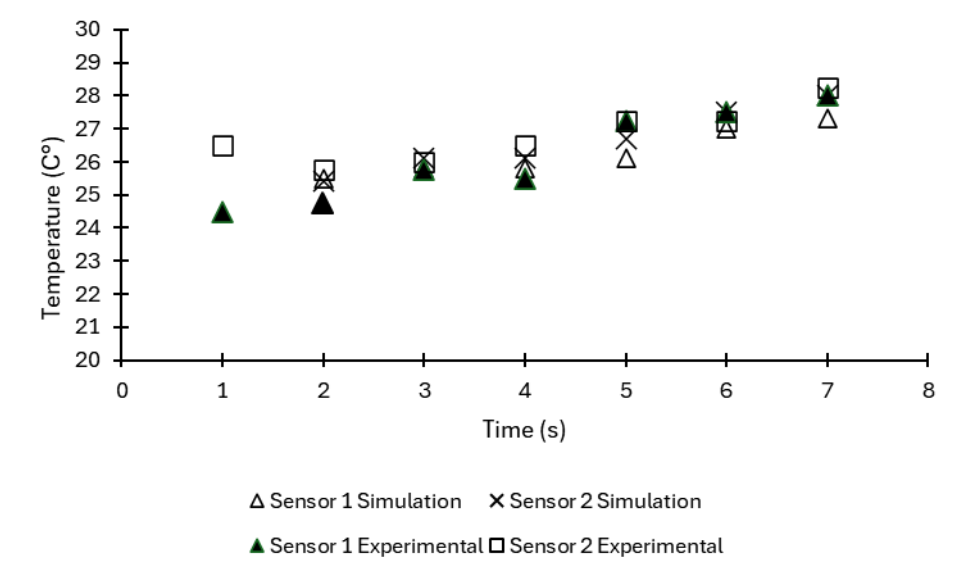

Figure 2. Comparison of experimental and simulated temperature profiles

In Figure 3a, the normalized velocity field $\boldsymbol{u}/\boldsymbol{u}_{\text{tip}}$ is shown in the mid-plane of the tank for the continuous phase (glycerin). The highest velocity magnitudes are concentrated in the immediate vicinity of the impeller, reflecting the transfer of mechanical energy from the impeller to the fluid. It is important to note that high-speed regions also coincide with high shear stress and viscous dissipation, which together produce intense local mixing (Martínez-de Jesús *et al*., 2018).

Figure 3b shows the flow pattern, where four main recirculation loops generated by the radial discharge of the impeller are clearly distinguished: two located in the upper region and two in the lower region. These patterns are characteristic of an impeller operating in the laminar flow regime. Identifying these vortices and recirculation zones not only provides insight into the internal hydrodynamics of the reactor but also establishes a solid foundation for optimizing operating conditions and guiding the design of more efficient stirred reactors.

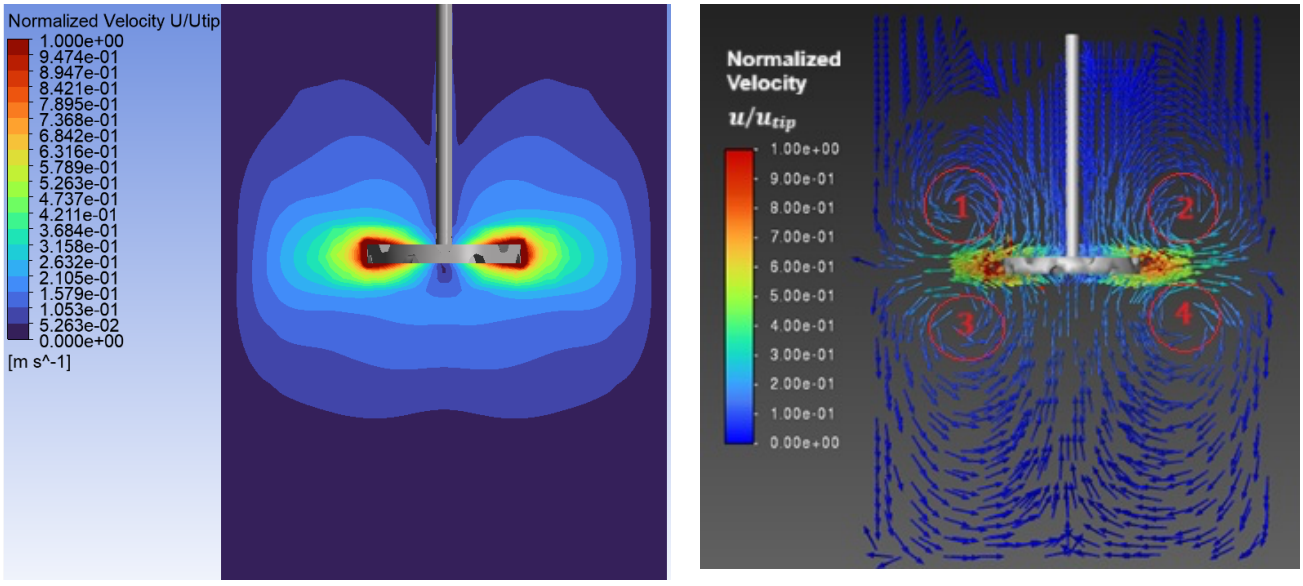

Figure 3. (a) Normalized velocity field of the entire reactor for the continuous phase (glycerin), (b) Normalized velocity vectors of the entire reactor for the continuous phase (glycerin)

Figure 4 depicts the evolution of the dispersed phase over time. The impeller surface is shown to be the primary site for hexane dispersion. Figure 5 shows the contour of the laminar viscous dissipation. The highest values (in red) are

concentrated around the impeller blades, particularly along the leading edges and in regions of greater curvature. This indicates that, in these areas, the mechanical energy supplied by the impeller is primarily converted into heat through shear stresses. In contrast, the regions between the blades and toward the central axis exhibit minimal dissipation (blue tones), demonstrating that the laminar contribution outside the impeller boundary layer is negligible. This information helps assess mixing efficiency, identify potential recirculation zones, and understand the initial generation of hydrodynamic instabilities. It also provides a basis for guiding improvements to the impeller and agitation system, promoting a more uniform distribution of energy throughout the reactor.

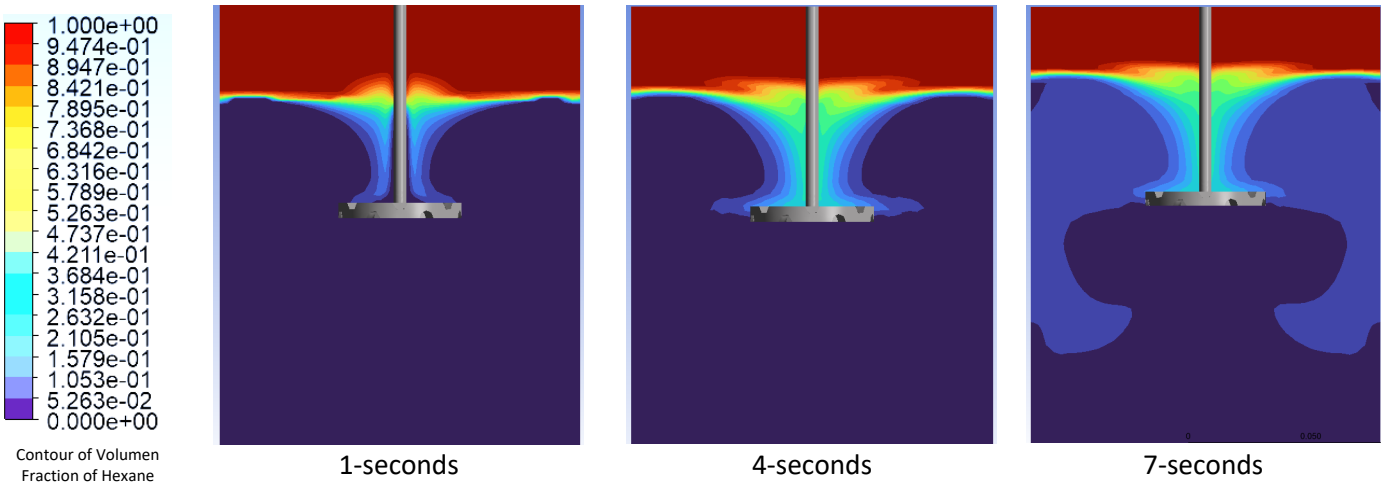

Figure 4. Phase contours corresponding to the dispersed phase (hexane)

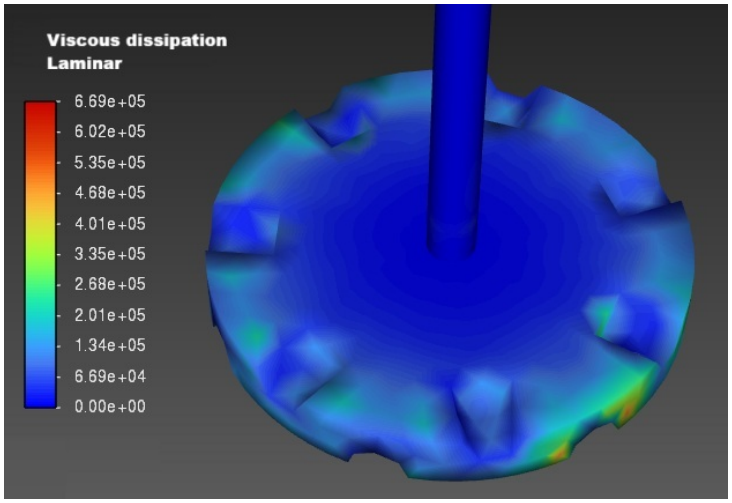

Figure5. Contours of laminar viscous dissipation

Conclusions

Computational Fluid Dynamics (CFD) simulations were utilized to characterize the hydrodynamic behavior of a Norstone-type high-shear impeller operating in a biphasic system. The analysis provided valuable insights into velocity fields, phase contours, and viscous dissipation contours, which are essential for understanding the dispersion of the secondary phase. The highest values for these parameters were observed in regions located near the impeller. To validate the numerical model, experimental temperature data were collected from strategically placed sensors. The strong agreement between the simulation results and the experimental data not only confirms the flow patterns predicted by the simulations but also validates the observed thermal variations. This combined approach of simulation and experimental analysis serves as a solid foundation for optimizing operating parameters in industrial processes. Consequently, these findings provide valuable insights for enhancing mixing efficiency in agitated tank systems handling biphasic flows, enabling more effective energy utilization and reduced processing times.

Acknowledgments and Funding: Gastón Martínez de Jesús and Adrián López Yáñez thank the support of COMECYT (Apoyo para estancias de investigación 2025)

Author contributions: J.A.P.-R.: writing – original draft, validation, investigation, formal analysis, conceptualization; A.L.Y.: writing – review & editing, investigation; R.A.A.C., M.I.N.-G. and A.M.-G.: writing – review & editing. G.M.-d.J.: writing – validation, investigation, formal analysis, conceptualization.

References

Andersson, B. (2012). *Computational fluid dynamics for engineers*. Cambridge University Press.

ANSYS, Inc. (2016). *ANSYS Fluent theory guide (Release 2016 R2)*.

ANSYS, Inc. (2024). *Ansys for students*. Ansys. https://www.ansys.com/academic/students

Deglon, D. A., & Meyer, C. J. (2006). CFD modelling of stirred tanks: Numerical considerations. *Minerals Engineering*, *19*(10), 1059–1068. https://doi.org/10.1016/j.mineng.2006.04.001

Jadhav, A. J., & Barigou, M. (2022). Eulerian–Lagrangian modelling of turbulent two-phase particle–liquid flow in a stirred vessel: CFD and experiments compared. *International Journal of Multiphase Flow*, *155*, 104191. https://doi.org/10.1016/j.ijmultiphaseflow.2022.104191

Martínez-de Jesús, G., Ramírez-Muñoz, J., García-Cortés, D., & Cota, L. G. (2018). Computational fluid dynamics study of flow induced by a grooved high-shear impeller in an unbaffled tank. *Chemical Engineering & Technology*, *41*(3), 580–589. https://doi.org/10.1002/ceat.201700091

Obando-Galicia, Y., Martínez-de Jesús, G., & Totosaus, A. (2024). Assisted (ultrasound or high shear impeller) soybean oil/lecithin extraction of polyphenolic compounds from red cactus pear peel: Extracts effects on oleogels properties. *Revista Mexicana de Ingeniería Química*, *23*(2), 1–11. https://doi.org/10.24275/rmiq/Alim24237

Oshinowo, L. M., Bakker, A., & Marshall, E. M. (2001). Virtual efficiency: Simulating mixing impellers using computational fluid dynamics. *Flow Control*, *7*(7), 28–33.

Steinmetz, M. (1993). *U.S. Patent No. 5,201,635*. U.S. Patent and Trademark Office. https://patents.google.com/patent/US5201635A/en

Stuparu, A., Susan-Resiga, R., & Bosioc, A. (2021). CFD simulation of solid suspension for a liquid–solid industrial stirred reactor. *Applied Sciences*, *11*(12), 5705. https://doi.org/10.3390/app11125705